Doctoral (Ph. D.) Theses

ELECTROCHEMICAL REDUCTION OF CARBON DIOXIDE ON GOLD-BASED BIMETALLIC ELECTRODES

Ahmed Mohsen Mohamed Ismail Mohamed

Supervisors:

Dr. Csaba Janáky

Associate Professor

Dr. Edit Csapó

Assistant Professor

DOCTORAL SCHOOL OF CHEMISTRY
University of Szeged
Faculty of Science and Informatics
Department of Physical Chemistry and Materials Science
Szeged

2020

1 Introduction and Aims

Traditional fossil fuels still occupy a remarkable position in today's energy structure. Carbon dioxide (CO_2) emissions generated via the combustion of fossil fuels lead to global climate change. Therefore, creating solutions to circumvent the intermittent nature of carbon-neutral energy sources, such as solar and wind, and decrease our dependence on fossil fuels is the most critical challenge facing humanity in the 21st century. CO_2 recycling (conversion) into valuable fuels and chemicals that can act as energy carriers is a promising route to create an artificial carbon cycle. Among different catalytic processes being developed for CO_2 recycling, the electrochemical CO_2 reduction reaction (CO_2RR) has attracted great attention as a promising step towards renewable energy utilization and storage. CO_2RR in an aqueous environment is rather complicated because of its substantial kinetic barriers compared to the competing hydrogen evolution reaction (HER). Therefore, developing electrocatalysts with high efficiency, selectivity, and long-term stability is a crucial step of great urgency towards industrialization.

It was very important to understand the activity and selectivity of pure metals before designing ***bimetallic nanoparticles*** *(NPs)*. Most metals catalyze the formation of 2 e^- reduction products (carbon monoxide (CO) and formic acid (HCOOH) with high Faradaic efficiency (FE)). Going beyond 2 e^- products is much more challenging as a result of the multiple proton and electron transfer steps. Through appropriate synthesis procedures, a wide range of combinations with various compositions, patterns of mixing, and intermetallic phases can be explored. Such bimetallic materials can provide active sites for the reaction intermediates with tunable binding strength and thus exhibit altered reactivity relative to their monometallic counterparts. The unique properties of the bimetallic catalysts arise from tailoring the electronic properties (shift of the Fermi level, E_F, with the respect to vacuum level) and the geometric effects, which stems from the atomic arrangement at the active sites. Au NPs selectively reduce CO_2 to CO due to the weak binding energy of *CO, which inhibits the further reduction to hydrocarbons and alcohols. Therefore, introducing a second metal with a different CO-binding energy, could effectively tune product distribution on Au-based catalysts. The combination of Au with Cu, Pt or Pd demonstrated that the catalytic properties of Au can be tuned, depending not only on the second metal but also on how Au was combined with the second metal.

Synthesis of bimetallic electrodes containing p-block metals (such as Sn, In and Pb, all having high H_2 overpotential and favor HCOOH production) is a good strategy not only to tune the CO_2RR activity and selectivity but also to suppress HER. Sn and Pb metals have been extensively mixed with Cu and showed a tunable selectivity between CO and HCOOH. Surprisingly, the combinations of Au with p-block metals were still lacking in the literature at the beginning of my doctoral studies.

Here, we aimed to provide a systematic study on the electrocatalytic activity of Au-based bimetallic NPs toward CO_2R. We carefully surveyed the literature and decided to explore the combination of Au with Sn, Pb, and Ag, as three bimetallic electrocatalysts which have not been employed in CO_2R yet. During my research, we aimed to find answers to the following questions:

- *Is it possible to combine Au with p-block metals, Sn and Pb, with different compositions?*
- *What is the structure (e.g., alloy, nanocomposite or new intermetallic phase) of these systems?*
- *How does the combination of p-block metals (Sn and Pb) with Au NPs affect the catalytic performance and product distribution?*
- *Is the native oxide layer of the p-block metals stable under the reduction conditions, and if yes, how does it affect the product distribution?*
- *Could the surface electronic properties alone determine the electrocatalytic performance of Au-Ag alloys?*

As a first step, our goal was to develop a direct and reproducible approach to synthesize Au-Sn NPs with tunable composition, and well-defined morphology. In the next step, we studied the catalytic activity of the Au-Sn NPs with different phase compositions. Further, we introduced a new synthetic approach to prepare Au-Pb catalysts to explore the effect of replacing Sn with Pb on the catalytic activity and product distribution. We also tried to uncover the role of Au/Pb interfaces in the electrocatalytic CO_2R as well as to elucidate the stability of the native sub-stoichiometric oxide under the reduction conditions. A series of Au-Ag alloy NPs with different compositions and narrow-size distribution was prepared, as a good model to investigate the correlation between the surface electronic properties and the catalytic activity in CO_2R.

2 Experimental Methods

Au-based bimetallic NPs with different compositions and uniform morphology were synthesized, showing three bimetallic systems with tunable structures (intermetallic phases, interfaces, and alloys). The main steps of the synthesis are depicted in **Figure 1**.

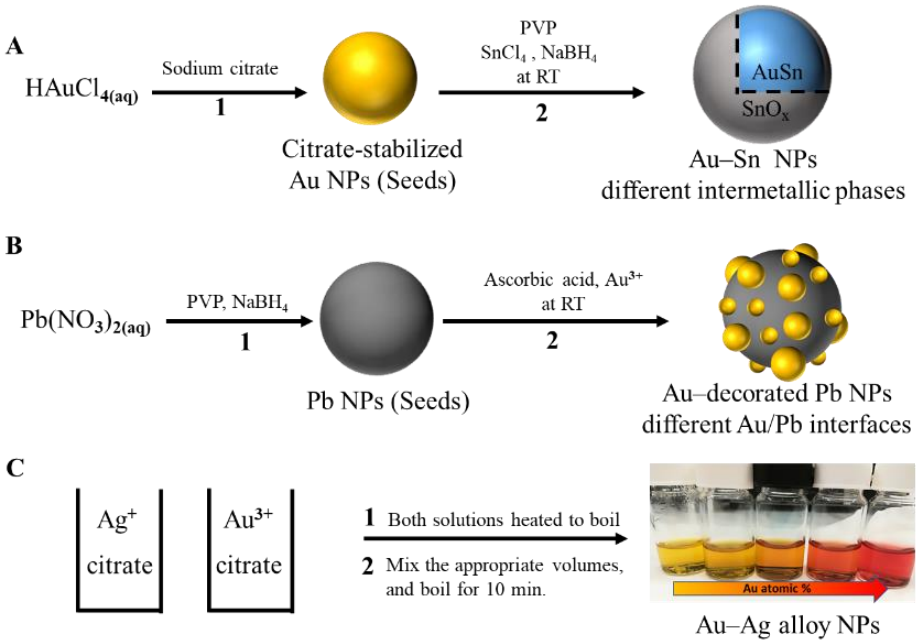

Figure 1. Schematic representation of the main steps of the synthesis of Au-based bimetallic NPs: (A) Au-Sn, (B) Au-Pb, and (C) Au-Ag

Morphology of the synthesized bimetallic NPs was studied by transmission electron microscopy (TEM). TEM images were taken by using compound FEI Tecnai G^2 20 X-Twin type instrument, operating at an accelerating voltage of 200 kV.

The bulk composition was analyzed with a Hitachi S-4700 field emission scanning electron microscope (SEM), operating at an accelerating voltage of 10 kV and equipped with an Energy-dispersive X-ray spectroscopy (EDX).

Powder X-ray diffraction (XRD) measurements were carried out to determine the crystal structure of the synthesized Au-based bimetallic NPs. The XRD patterns were obtained by a Bruker D8 advance instrument with Cu Kα (λ = 1.5418 Å) radiation, in the 2-theta range of 10-80°, with a scan rate of 0.4° min^{-1}.

The X-ray photoelectron spectroscopy (XPS) was performed with a PHOIBOS 150 MCD 9 hemispherical analyzer. Charge neutralization was carried out during spectra acquisition, where the position and width of the adventitious carbon peak were monitored. The adventitious carbon peak was at 284.8 eV in all cases.

The Au-Sn and Au-Pb catalysts were dispersed in isopropanol (5 mg cm^{-3}) and spray-coated to a preheated glassy carbon electrode, using an Alder AD320 type airbrush and a homemade spray-coater robot, operated with 1 bar compressed nitrogen. For the Au-Ag electrodes, a concentrated dispersion of the prepared Au-Ag alloys was drop-casted to a preheated (80 ^{o}C) glassy carbon electrode. The precise loading of the catalyst was monitored by a Mettler Toledo XPE-26 type analytical microbalance.

All electrochemical measurements were carried out with a Metrohm Autolab PGSTAT302 type potentiostat/galvanostat in a standard three-electrode setup. The bimetallic catalyst on glassy carbon electrodes functioned as the working electrode. A platinum foil (Alfa Aesar, 99.99%) and Ag/AgCl (3 M NaCl) were used as a counter electrode and a reference electrode, respectively. The measured potentials were converted to reversible hydrogen electrode (RHE) reference scale using $E_{RHE} = E_{Ag/AgCl} + 0.210\ V + 0.0591 \times pH$. Linear sweep voltammetry (LSV) and cyclic voltammetry (CV) profiles were recorded in a sealed, custom-designed one-compartment cell.

CO_2 electrolysis experiments were carried out in a gastight two-compartment electrochemical cell to characterize the catalytic performance. A Nafion-117 proton exchange membrane was used as the compartment separator. Each compartment was filled with a bicarbonate (HCO_3^-) solution, which was purged with CO_2 gas before the electrolysis for 30 min. During chronoamperometry measurements, the effluent gas from the headspace of the cathodic compartment was fed into the online sampling loop of the gas chromatograph (GC) every 30 min for quantification of gas-phase CO_2 reduction products. The GC (SHIMADZU, GC-2010 plus) was equipped with a barrier discharge ionization detector. The liquid sample was collected at the same time and analyzed using a Bruker Avance Neo 500 NMR spectrometer. The sample (450 µL) was mixed with 50 µL D_2O containing phenol and dimethyl sulfoxide as internal standards. The one-dimensional ^1H spectrum was measured using a solvent presaturation method to suppress the water peak. FE values of the products were calculated from the amount of charge passed to produce each product divided by the total charge passed.

Isotopic labeling experiments were performed where both carbon sources (CO_2 gas and HCO_3^-) were labeled. GC–MS (Shimadzu GC-MS QP2010 S, RT Molsieve 5 Å column) was employed for monitoring the isotopic composition of the CH_4 and CO Products, in selective ion monitoring mode. A gas sample of 300 µL was taken from the headspace of the cathodic compartment and injected into the GC–MS with a gastight syringe every 11 min. And $H^{13}COOH/H^{12}COOH$ ratio deduced from NMR results.

In situ Raman spectroelectrochemical experiments were performed using an ECC-Opto-Std electrochemical cell (EL-CELL GmbH) equipped with a sapphire window, and a potentiostat/galvanostat (Interface 1010E – GAMRY). Raman spectra were recorded after a 100 s potentiostatic conditioning at each potential with a SENTERRA II Compact Raman microscope, using 532 nm laser excitation wavelength by 2.5 mW power and a 50× objective.

Kelvin probe microscopy-coupled ambient pressure UV-photoelectron spectroscopy (APS) measurements were conducted using a KP Technology APS04 instrument. First, the contact potential difference was measured between the sample and a 2 mm-diameter tip with gold alloy coating after electric equilibrium was reached. APS measurements were carried out with a stationary Kelvin-probe tip.

Density functional theory (DFT) calculations were performed with VASP 5.4.4, the Perdew−Burke−Eenzerhof functional was used with projected augmented wave pseudopotentials and an energy cutoff the plane waves of 450 eV. to support the proposed mechanism of CH_4 formation on Au-Pb surface. The theoretical study was carried out by the research group of Prof. Núria López (ICIQ Tarragona, Spain), and we had regular meetings to discuss their theoretical efforts. All structures and input and output files can be accessed at the ioChem-BD database under this link: https://iochem-bd.iciq.es/browse/review-collection/100/22849/0ed1c88f8d705d4306cea07d

3 Summary of New Scientific Results

T1. We provided a strategy to synthesize Au-Sn electrocatalysts with a bimetallic core and an ultra-thin partially oxidized SnOx shell. This two-step approach was demonstrated by a series of spherical-shaped Au-Sn nanoparticles with a narrow size distribution and tunable composition. Two intermetallic phases (AuSn and $AuSn_2$) were formed.

Au-Sn NPs with different nominal compositions (i.e., Au_2Sn_1, Au_1Sn_1, Au_1Sn_2, and Au_1Sn_4) were successfully synthesized by the chemical reduction of different amounts of Sn precursor in the presence of the premade Au seeds at ambient conditions. The size of the particles was 23 ± 2.9, 31.8 ± 3.9, 32.4 ± 3.7, and 33 ± 2.5 nm, in the series of samples with increasing Sn content. The AuSn intermetallic phase became more prevalent with increasing Sn^{4+} concentration, achieving 100% at the Au_1Sn_2 sample. $AuSn_2$ intermetallic.phase was observed at the highest Sn content (sample Au_1Sn_4). The amount of the partially oxidized tin species (SnO_x) at the surface increased gradually with the total Sn concentration, and there was no sign of oxidized Au.

T2. The phase composition influences the electrocatalytic activity of Au-Sn NPs in CO_2R. While two high-value products (HCOOH and syngas) were formed in all cases, their ratio was dependent on the composition. The catalyst with the AuSn phase showed the lowest overpotential compared to pure Au and Sn NPs as well as their physical mixture.

LSV profiles of the different Au-Sn electrodes showed that the onset potential values span through 440 mV, and the trend does not reflect the change in the composition. This confirms the formation of new intermetallic phases (rather than simple alloying), which in turn results in a non-linear change in the bulk and surface energetics, dictating the CO_2 reduction properties. The bimetallic samples outperformed both gold and tin and showed a good product distribution. The Au_1Sn_2 catalyst (containing almost pure AuSn phase) showed the lowest overpotential for CO_2R, 400 mV less negative compared to pure Sn. At – 1.0 V vs. RHE, a current of 8 mA cm^{-2} was achieved and remained stable for 10 h.

T3. Isotope labeling experiments proved that CO_2 molecules generated via the fast equilibrium with the bicarbonate ions, are the primary source of the produced reduction products. In situ Raman spectroelectrochemistry confirmed the generation of formate anions on the AuSn phase at a notably less negative potential compared to pure Sn electrode as well as the stability of SnO_x layer under the reaction conditions.

Selective isotopic labeling experiments were performed under nonequilibrium condition, suggesting that CO_2 supplied through fast equilibrium with the bicarbonate, rather than CO_2 in the bulk solution, is the primary source of the produced CO and HCOOH. In situ Raman spectroelectrochemistry confirmed the presence of bicarbonate anions on the electrode surface and the stability of SnO_x under the reaction conditions and proved the generation of formate anions at a notably less negative potential on the AuSn phase (− 0.59 V vs. RHE) compared to the pure Sn electrode (− 0.92 V vs. REE).

T4. Au-decorated Pb NPs were synthesized with uniform morphology and various compositions using a controlled galvanic replacement method. This process allowed to tune the composition and thus the relative amount of Au/Pb interfaces. An inverse structure, Au core- Pb-shell NPs were also prepared with a similar composition and crystal structure.

A series of Au-decorated Pb NPs (i.e., Au_5Pb_{95}, $Au_{20}Pb_{80,}$ $Au_{50}Pb_{50}$) was successfully synthesized with the same size and different Au/Pb interfaces. The first step is the formation of metallic Pb NPs, followed by the galvanic displacement of Pb with Au. TEM images depict well-distributed Au dots on the surface of the Pb particles. The increase of Au content results in higher coverage. Au-core -Pb-shell ($Pb_{95}Au_5$) NPs were also prepared with a similar composition to the most Pb-rich sample (Au_5Pb_{95}). XRD study showed that the intensities of Pb, PbO, and PbO_2 peaks decreased notably with increasing Au concentration to 20 %, while the Au phase became more prevalent without a shift in the reflection positions, suggesting that the majority of the Pb species are present in an amorphous phase (e.g., non-stoichiometric oxide) and these bimetallic samples are particles containing nanosized domains of both metals.

T5. Au-Pb bimetallic catalysts with different Au/Pb interfaces work synergistically to transform CO_2 to a > 2 e^- reduction product (CH_4). The chemically stable PbO_x and Au are crucial to provide the proper sites along the pathway for the CO_2 conversion to CH_4, CO, and HCOOH. The role of the Au/Pb interfaces in the electrocatalytic activity and selectivity was found to be necessary.

CH_4 (together with CO and HCOOH) was generated on Au/Pb electrodes. On Au, Pb, or their physical mixture only trace amounts of CH_4 was detected, and the stability of PbO_x under the reduction condition was high on the bimetallic catalyst (unlike for bare Pb) which seems to be necessary for CH_4 formation, and further proving our notion on the role of nanoscale interfaces. DFT calculations confirmed that the Au/Pb bimetallic interface, together with the subsurface oxygen possess a moderate binding strength for the key intermediates, which is indeed necessary for the CH_4 pathway. Experimental results indicated that comparable amounts of Au and Pb are needed at the surface to ensure high reaction rates.

T6. A series of monodisperse Au-Ag nanoalloys were prepared in the 25-30 nm range, with different compositions and uniform morphology. Tunable plasmonic properties were demonstrated, where the localized surface plasmon resonance band red-shifted in a linear fashion with increasing the Au content. Ag@Au core-shell NPs were successfully prepared with similar size and composition for comparative studies.

Au-Ag NPs with different compositions (i.e., $Au_{80}Ag_{20}$, $Au_{60}Ag_{40}$, $Au_{40}Ag_{60}$ and $Au_{20}Ag_{80}$) were synthesized. The particles are spherical, and the average size increased from 24.5 ± 1.8 to 26.6 ± 2.4, 31.5 ± 1.3, and 32.1 ± 3.8 nm, in the series of the samples, as the amount of Ag increased. The average size of the core-shell NPs is 29.2 ± 4.2 nm which is similar to their alloyed counterparts. The Au-Ag alloy NPs show only one absorption band for each composition, located in between the plasmon band positions of Au and Ag NPs.

T7. The electronic properties of Au-Ag alloy electrocatalysts were tuned with the composition, while keeping other structural parameters fixed. The Fermi level shifts

downwards linearly between 4.68 eV and 4.49 eV with the Au content, which was consistent with the observed trend of electrocatalytic properties (j_{CO}increases with Au content).

There was a monotonous shift in the onset potential of CO_2R in the series of samples, which spans through a 300 mV range. CO and H_2 were the major products for all electrodes. FE_{CO} increased from 42% to 60% with increasing Au content, while the FE of H_2 evolution simultaneously decreased. This indicates that the CO:H_2 ratio can be tuned by controlling the bimetallic composition. The j_{CO} increased gradually showing a similar trend to that observed for the E_F.

T8. The CO_2R activity of Ag@Au core-shell NPs was compared to that of nanoalloy (similar bulk composition) and pure Ag (similar electronic structure). Substantial differences were revealed in both comparisons, both the selectivity and the activity. These trends indicated that neither electronic nor geometric effect *alone* can determine the electrocatalytic properties.

Ag@Au core-shell catalyst generates CO with a FE of 68.7 %, versus 45.0% at −0.7 V vs. RHE for alloy ($Au_{20}Ag_{80}$) NPs of the same bulk composition. Compared to pure Ag, the Ag@Au with Ag shell (similar electronic structure) indicated differences in both activity and product distribution (68.7 % versus 25 % for FE_{CO}. at −0.7 V vs. RHE). This indicates that both the electronic and geometric effects need to be considered during the bimetallic catalyst for selective and efficient CO_2 reduction.

4 List of Publications

Hungarian Scientific Bibliography (MTMT) identifier: 10071976

Publications related to the scientific topic of the dissertation

1) **Ahmed Mohsen Ismail**, Gergely F. Samu, Ádám Balog, Edit Csapó, and Csaba Janáky
   Composition-Dependent Electrocatalytic Behavior of Au–Sn Bimetallic Nanoparticles in Carbon Dioxide Reduction
   ACS Energy Lett. **2019**, *4*, 48–53. doi:10.1021/acsenergylett.8b01996
   IF_{2018} = 16.331

2) **Ahmed Mohsen Ismail**, Edit Csapó, and Csaba Janáky
   Correlation between the Work Function of Au–Ag Nanoalloys and Their Electrocatalytic Activity in Carbon Dioxide Reduction
   Electrochim. Acta **2019**, *313*, 171–178. doi:10.1016/j.electacta.2019.05.016
   IF_{2018} =5.383

3) **Ahmed Mohsen Ismail**, Gergely F. Samu, Huu Chuong Nguyën, Edit Csapó, Núria López, and Csaba Janáky
   Au/Pb Interface Allows the Methane Formation Pathway in Carbon Dioxide Electroreduction
   ACS Catal. **2020**, *10*, 5681–5690. doi:10.1021/acscatal.0c00749
   IF_{2018} = 12.221

$\sum$IF = 33.935

Conference Lectures and Posters

Lecture:

1) **Ahmed Mohsen Ismail**, Gergely F. Samu, Edit Csapó, and Csaba Janáky
   Electrochemical CO_2 Reduction at Different Au-Sn Bimetallic Catalysts
   International Symposium on Electrocatalysis (Electrocat2018)
   29 August – 1 September, 2018, Szczyrk, Poland

2) **Ahmed Mohsen Ismail**, Gergely F. Samu, Edit Csapó, and Csaba Janáky
   Au-Sn Bimetallic Electrocatalysts for Electrochemical CO_2 Reduction
   8th Szeged International Workshop on Advances in Nanoscience (SIWAN 8)
   7 – 10 October, 2018, Szeged, Hungary

3) **Ahmed Mohsen Ismail**, Edit Csapó, and Csaba Janáky
   Bimetallic electrocatalysts for electrochemical CO_2 reduction
   International symposium intermetallic Compounds in Catalysis (IMCAT 2019)
   17 – 19 September, 2019, Chemnitz, Germany

Posters:

1) **Ahmed Mohsen Ismail**, Gergely F. Samu, Edit Csapó, and Csaba Janáky
   Composition Dependent Electrocatalytic Behavior of Sn-Au Bimetallic Nanoparticles in Carbon-dioxide Reduction
   69th Annual Meeting of the International Society of Electrochemistry
   2 – 7 September, 2018, Bologna, Italy

2) **Ahmed Mohsen Ismail**, Edit Csapó, and Csaba Janáky
   Au-Ag Bimetallic Catalysts with Different Composition for CO2 Reduction
   International Workshop on Electrochemistry of Electroactive Materials (WEEM – 2019)
   16 – 21 June, 2019, Borovets, Bulgaria

3) **Ahmed Mohsen Ismail**, Edit Csapó, and Csaba Janáky
   Bimetallic electrocatalysts for electrochemical CO_2 reduction
   International symposium intermetallic Compounds in Catalysis (IMCAT 2019)
   17 – 19 September, 2019, Chemnitz, Germany

Co-author of conference posters

1) Edit Csapó, Ditta Ungor, Ádám Juhász, Csaba Janáky, **Ahmed Mohsen Ismail**
   Noble metal colloids: development of optical sensors and electrocatalysts
   8th International Workshop on Advances in Nanoscience (SIWAN 8)
   7– 10 October, 2018, Szeged, Hungary

2) Edit Csapó, Ditta Ungor, Ádám Juhász, Csaba Janáky, **Ahmed Mohsen Ismail**
Size-controlled noble metal colloids and clusters: development of electrocatalysts and optical biosensors
9th International Colloids Conference (COLL2019)
16 – 19 June, 2019, Barcelona-Sitges, Spain